Constitutive Model for Tailing Soils Subjected to Freeze-Thaw Cycles Based on Meso-Mechanics and Homogenization Theory

Youneng Liu[1], Enlong Liu[2, 3*], Zhenyu Yin[4]

(1. Institute for Disaster Management and Reconstruction, Sichuan Univ., Chengdu 610207, China; 2. State Key Laboratory of Hydraulics and Mountain River Engineering, College of Water Resource and Hydropower, Sichuan Univ., Chengdu 610065, China; 3. Northwest Institute of Eco-Environment and Resources, State Key Laboratory of Frozen Soil Engineering, Chinese Academy of Sciences, Lanzhou 730000; 4 Department of Civil and Environmental Engineering, The Hong Kong Polytechnic University, Hung Hom, Kowloon, Hong Kong）

*Corresponding author: Enlong Liu; Email: liuenlong@scu.edu.cn; Tel: +86 28 85400398.

Abstract

A constitutive model is proposed for tailing soils subjected to freeze-thaw cycles based on the meso-mechanics and homogenization theory. The evolution of meso-structure upon loading was analyzed within the framework of breakage mechanism. When the new model is formed, tailing soils are idealized as composite materials composed of bonded elements described by an elastic brittle model and frictional elements described by a double hardening model. Based on meso-mechanics and homogenization theory, the nonuniform distributions of stress and strain within the representative volume element are given by introducing a structure parameter of breakage ratio with the derivation of the strain coefficient tensor, which connects the strains of the bonded elements and the representative volume element. The methods for determining model parameters are suggested based on the available tested results. The model proposed here can predict the deformation properties of tailing soils experiencing freeze-thaw cycles

with acceptable accuracy. The strain-hardening and post-peak strain-softening behaviors of tailing soils under various confining pressures as well as different numbers of freeze-thaw cycles are well captured, and the dilatancy and contraction features are also adequately represented.

Keywords: Constitutive model; Tailing soils; Freeze-thaw cycles; Meso-mechanics; Homogenization theory

1. Introduction

Tailing soils discharged from mineral processing are appreciably distinct from general soils in terms of size, shape and physical and chemical properties. To dispose of these mining residues, the current practice is to pump the tailings slurry into storage facilities resisted by embankments, which are constructed out of the tailing soils themselves. It was reported in the literature that China held approximately 12 thousand tailings pounds up to 2012 [7], and 91.4% of these tailings storage facilities were located in the cold regions [42], effectively most of which were distributed in seasonally frozen regions. When the hydraulic filling method is applied during construction, a loose structure with a high level of the phreatic line will be easily formed inside the tailings dykes because of the smaller size of tailings. Particularly, those saturated tailings dykes in seasonally frozen regions can be intensely impacted by the frost heave and thawing settlement, in a consequence, the strength deterioration of tailing soils will occur during freeze-thaw cycles. In addition, tailings storage facilities are complexes with high potential energy, large scale and poor stability. Once collapsing, it would pose a big threat to the people and the ecological environment downstream. Hence, in order to guarantee the safety and stability of the tailings dam in cold regions, it is essential to assess the mechanical properties and formulate constitutive models of tailing soils subjected to the freeze-thaw cycles.

Up to the present, considerable efforts have been devoted on the mechanical properties of tailing soils by laboratory experiments [1, 4, 5, 12, 16, 32, 43, 50], in which the mineral composition, microstructure, strength and deformation properties, dewatering treatment, and static and seismic liquefaction of tailing soils were investigated. It is considered that during the freeze-thaw cycles, the water migration and phase transformation can occur under the temperature gradient, leading to a microstructure adjustment inside geological materials, consequently, it may cause heterogeneity in tailing soils and result in a property deterioration in macroscale [15, 25, 51]. Frozen temperature is a crucial factor that impacts the amount of freezable water within soils and influences the rate of freezing, which will affect the formation of ice lenses and influence the soil structure [29, 33]. When subjected to freeze-thaw cycles, the supercooling phenomenon and the hysteresis effect of volumetric unfrozen water content were both observed in fine soils [49]. And different frozen temperature can lead to a contrary volumetric behavior [46]. A series of molecular dynamics simulations were conducted by Zhang [47] to investigate the adsorption and un-freezable threshold of porous materials, where an explicit mathematical equation has been suggested to predict the melting temperature in cylindrical pores. On the contrary, other research suggests that the influence of frozen and melting temperatures is insignificant on the water migration and its phase transformation, as long as the frozen temperature drops below -4℃ and rises above 0℃, respectively [8].

It was demonstrated in a number of studies that the interstitial mineral particles can be squeezed up with the growth of ice crystals, as a result, the mean pure size of tailing soils will expand during the subsequent thawing process, and the internal water experiences enhanced permeability and seepage could occur under gravity. Consequently, there will be an overall decrease incompressibility and volume of tailing soils [2, 31, 37]. However, it should be noted that the improvement on the dewatering conditions and the strength under freeze-thaw treatment has been reported only in sludge tailing soils.

On the contrary, other researches recommended that tailing soils as artificial materials are more complex in components when compared with natural geological materials, because they generally contain some crystal water, metal oxides and some other unstable compounds [24, 44], which may break up when experienced freeze-thaw cycles or upon loading. It is also considered that during the freeze-thaw cycles, the growth of ice crystals can cause a loose structure in tailing soils, which means an increase on void size and a decrease on density, as a result, the strength of tailing soils will significantly decline after freeze-thaw cycles [45].

It was suggested in the previous studies that under relative low confining pressures with the increasing numbers of freeze-thaw cycles, the stress-strain relationship of natural soft clay will transform from stain-softening behavior to strain hardening behavior, even the post-peak reduction on deviatoric stress was not noticeable in the strain-soften behavior [38, 39]. By contrast, both loose sand and coarse-grained soils generally present strain-hardening behavior under various confining pressures and different numbers of freeze-thaw cycles [11, 22]. However, due to breakage properties, tailing soils are distinct from natural soils in terms of stress-strain relationships, which tend to present a significant post-peak strain-softening behavior under low confining pressure, and it is significantly affected by freeze-thaw cycles.

Much work so far has been focused on the non-linear deformation behavior of soils subjected to freeze-thaw cycles, and some widely adopted methods involve revising or reformulating Duncan-Chang model [18], elasto-plasticity model [9, 11, 17], and damage mechanical model [10, 41]. However, some of these models are formulated based on the macroscopic observations of the stress-strain properties, and few of them consider the heterogeneous distributions of stress and strain in geological soils. Based on the mesoscopic profile and the composite mechanics theory, Liu [23] proposed a serial model and a parallel model, and a corresponding transversely isotropic frost heave modeling was then developed, which was applied in the simulation of the frost heave problems. Similar to the soil-water characteristic curves for unsaturated soils, ice-water characteristic curves for frozen soils were suggested and applied in developing a coupled heat and fluid transfer model [3]. The model is used in investigating the fluid flow in partially frozen ground. So far, very little information is available about constitutive models for tailing soils, especially for tailing soils subjected to freeze-thaw cycles. And thus, the current practice that uses conventional constitutive models in stability analysis for tailings dams [6, 27, 28] cannot capture the fundamental distinctions between tailing soils and other geological materials, what's more, it might cause highly inaccurate predictions because of the difference in meso-scale aspect of failure mechanism. Therefore, to improve the capability of disaster prevention and safety evaluation for tailings dam in cold regions, it is essential to consider the breakage mechanism of tailing soils and to further formulate proper constitutive models incorporated with the influence of freeze-thaw cycles.

To describe the heterogeneous distributions of stress and strain on geological materials, Shen [34, 36] proposed a so-called breakage mechanics theory, in which the geological materials are idealized as composites consisted of bonded elements and frictional elements. However, in the previous studies [20, 34, 36, 48], the strain coefficient tensor L_{ijkl} (or a similar stress coefficient tensor) connecting the strains (or stress) between bonded elements and representative volume element was given by an assumed symmetry matrix $\left[L_{xy}\right]$ and determined though fitting with test results, which may not well agree with the complicate properties of geological materials. In the present study, the breakage mechanism under loading and freeze-thaw cycles is discussed. Besides, an Eshelby-form tensor is introduced, and thus the strain coefficient tensor L_{ijkl} is derived mathematically based on meso-mechanics and homogenization theory. Furthermore, a new constitutive model, referred to as the binary-medium model, is formulated with consideration of the breakage process and nonuniform distribution of stress (or strain). The predicted results and experimental data of tailing soils are compared and the salient features of the proposed model are discussed.

2. Formulation of the constitutive model for tailing soils subjected to freeze-thaw cycles

2.1 Breakage mechanism of tailing soils subjected to freeze-thaw cycles

Within the theory of breakage mechanics for geological materials [34, 36], the shear strength of geological materials is considered to be composed of cohesive resistance and frictional resistance, in which the former exhibits brittle behavior and the latter exhibits nonlinear behavior. And thus, geological materials are idealized as binary-medium materials composed of bonded elements and frictional elements, corresponding to the cohesive resistance and frictional resistance, respectively. A schematic diagram of the binary-medium structure is shown in Fig. 1, where a bonded element is an elastic-brittle structure composed of a brittle bond (b) and a spring (E_b), and a frictional element is an elastoplastic medium consisted of a plastic slider (f) and a spring (E_f). A structural unit of geological material can be assumed as a continuum body containing many bonded elements and frictional elements, as shown in Fig. 1 (a). With the gradual breaking of the brittle bonds upon loading, the bonded elements transform to elastoplastic frictional elements, hence the two components contribute to the bearing capacity collectively.

For tailing soils, the existence of crystal water, activating oxides and some other unstable compounds makes it present a complex behavior upon loading, as the crystal water, unstable compounds and the skeleton of tailing soil grains bear external loads collectively. In addition, activating oxides, for instance,

SiO_2, Al_2O_3, Fe_2O_3 and CaO can transform to cement substances when immersed into water, which provides a strong cohesive force. In order to consider these heterogeneous properties, tailing soils here are idealized as quasi-continuous mediums composed of many binary-medium structures based on the theory of the breakage mechanics. The bonded elements are represented by the soil aggregate structures containing crystal water, unstable compounds and cement, while a frictional element is regarded as an aggregate structure, which is transformed from a bonded element after an entire breakage of the inside crystal water, unstable compounds and cement.

The bonded elements and frictional elements of tailing soils bear the external loading collectively, however, their contributions for the resistance vary with the total strain or deformation level [19]. The bonded elements make a full contribution within a relatively smaller strain level but the frictional elements almost carry the whole external loading at a relatively larger deformation or strain level. Here, two typical stress-strain relationships of tailing soils [24] are discussed, as shown in Fig. 2, where (a) presents a strain-hardening behavior and (b) shows a strain-softening behavior, and both types of tested results are divided into three segments. Within a small strain level on line 0A where the crystal water, unstable compounds and cement are hardly broken, the bonded elements in both patterns stay at an elastic level. Meanwhile, the external loads at this stage are primarily borne by the bonded elements, and thus both types of tested results present a linear stress-strain relationship with a high deformation modulus. As the development of axial strain, the tested results get into line AB, where the stress-strain behavior of both types becomes non-linear and turns into an elastoplastic stage, accompanied by a gradual decrease in tangential deformation modulus. At this stage, the initial damage is generated and begins developing inside the crystal water, unstable compounds and cement owing to the stress concentration, which aggravates the breakage process of the brittle bonds. Hence with the increasing strain, the bonded elements gradually break and transform to frictional elements, and the strength loss due to breakage is compensated by the newly generated frictional elements. And tailing soils ultimately can present a strain-hardening behavior or a strain-softening behavior, depending on whether the compensation effect of frictional elements is strong or weak, as shown in Line segment BC in both Figure 2 (a) and (b). In addition, the strain-hardening behavior of tailing soils always takes place accompanied by volume compression, and strain-softening behavior often occurs with a volume compression at initial loading followed by a volume dilatation.

In the current study, tailing soils composed of mineral particles, crystal water, unstable compounds and cement are idealized as binary-medium materials. In order to investigate their failure mechanism, a representative volume element (RVE) of binary-medium structures is defined and analyzed in this section. To guarantee that the average stress and average strain of the RVE are consistent with the overall tailing soil structure, the RVE should be chosen smaller enough compared with the overall volume of the tailing soil specimen and also should simultaneously contain adequate meso-structure information. Therefore, a RVE is extracted from an assumed quasi-continuum tailing soils sample, as shown in Fig. 3, where the soil particles are idealized to be spherical. In a binary-medium structure, a bonded element Ω^b is defined as a spherical collection of soil grains where the voids are occupied with crystal water, unstable compounds and cement. These filling materials are regarded as brittle bonds which possess a strong cohesive resistance. The elastic bonded element can convert into an elastoplastic frictional element Ω^f after an entire breakage of its brittle bond.

In the current formulation, all stresses used are effective stresses, and the superscript b and f denote a variable of bonded elements and frictional elements, respectively. The variables are defined with tensor by using a generalized three-dimensional Cartesian coordinate system $(\mathrm{X}_j, j = x, y, z)$, where the

Einstein summation convention is adopted over the repeated indices in the notations.

2.2 The local strain coefficient tensor

In this section, the meso-mechanic theory is introduced in order to derive the local strain coefficient tensor A_{ijkl}, who bridges the strain of bonded elements and frictional elements. As the RVE shown in Fig. 3, the bonded elements and frictional elements are regarded as inclusions and matrix materials based on meso-mechanics, respectively.

The bonded elements are assumed to have elastic property within the critical strain level, and their stress-strain relationship can be incrementally expressed as follows:

$$\mathrm{d}\sigma_{ij}^{b} = D_{ijkl}^{b}\mathrm{d}\varepsilon_{kl}^{b} \tag{1}$$

and

$$D_{ijkl}^{b} = {}^{1}\!/_{3}\,(3K^{b} - 2G^{b})\delta_{ij}\delta_{kl} + G^{b}\left(\delta_{ik}\delta_{jl} + \delta_{il}\delta_{jk}\right) \tag{2}$$

where D_{ijkl}^{b} is the tensor of elastic modulus of bonded elements; σ_{ij}^{b} and ε_{ij}^{b} are the average stress and average stain increments of bonded elements, respectively; K^{b} and G^{b} denote the bulk modulus and shear modulus of bonded elements, respectively; δ_{ij} is denoted by Kronecker delta, (i.e., $\delta_{ij} = 1$ if $i = j$, and $\delta_{ij} = 0$ if $i \neq j$).

The frictional elements compose the matrix of RVE, and they present elastoplastic property, with the constitutive relationship expressed as:

$$\mathrm{d}\sigma_{ij}^{f} = D_{ijkl}^{f}\mathrm{d}\varepsilon_{kl}^{f} \tag{3}$$

and

$$D_{ijkl}^{f} = D_{ijkl}^{fe} - \frac{D_{ijmn}^{fe}\left\{\dfrac{\partial g}{\partial \sigma_{mn}}\right\}\left\{\dfrac{\partial \phi}{\partial \sigma_{pq}}\right\}^{\mathrm{T}} D_{pqkl}^{fe}}{H + \left\{\dfrac{\partial \phi}{\partial \sigma_{ij}}\right\}^{\mathrm{T}} D_{ijkl}^{fe}\left\{\dfrac{\partial g}{\partial \sigma_{kl}}\right\}} \tag{4}$$

where D^{f}_{ijkl} is the tangential elastoplastic modulus tensor of the frictional elements; $\mathrm{d}\sigma^{f}_{ij}$, $\mathrm{d}\varepsilon^{f}_{ij}$, ϕ, g and H denote the average stress increment, average stain increment, yielding function, plastic potential function and Hardening modulus of the frictional elements, respectively; and

$$D^{fe}_{ijkl} = {}^{1}\!/_{3}\,(3K^{fe} - 2G^{fe})\delta_{ij}\delta_{kl} + G^{fe}\left(\delta_{ik}\delta_{jl} + \delta_{il}\delta_{jk}\right) \tag{5}$$

where K^{fe} and G^{fe} denote the elastic bulk modulus and shear modulus of the frictional elements, respectively.

In classical soil plasticity, the average stain increment $\mathrm{d}\varepsilon^{f}_{ij}$ of elastoplastic frictional elements are usually decomposed into recoverable elastic component $\mathrm{d}\varepsilon^{fe}_{ij}$ and irrecoverable plastic component $\mathrm{d}\varepsilon^{fp}_{ij}$ as the following expression:

$$\mathrm{d}\varepsilon^{f}_{ij} = \mathrm{d}\varepsilon^{fe}_{ij} + \mathrm{d}\varepsilon^{fp}_{ij} \tag{6}$$

In the current study, the modulus D^{b}_{ijkl}, D^{f}_{ijkl} and D^{fe}_{ijkl} are assumed to be incrementally linearized during the loading process.

Suppose an RVE is fully occupied with frictional elements, and an eigenstrain increment $\mathrm{d}\varepsilon^{*}_{ij}$ is generated in an ellipsoidal area Ω of the RVE, as shown in Fig. 4 (a), thus an Eshelby-form tensor S^{ep}_{ijkl} could be employed to bridge the constrained strain increment $\mathrm{d}\varepsilon^{t}_{ij}$ and the given eigenstrain increment $\mathrm{d}\varepsilon^{*}_{ij}$ among the ellipsoidal area Ω, with the following definition:

$$\mathrm{d}\varepsilon^{t}_{ij} = S^{ep}_{ijkl}\mathrm{d}\varepsilon^{*}_{kl} \tag{7}$$

where the Eshelby-form tensor S^{ep}_{ijkl} has been given by the following expression [30]:

$$S^{ep}_{ijkl} = [(D^{fe}_{ijmn})^{-1}D^{f}_{mnop}]^{-1}S_{opqr}\left[(D^{fe}_{qrst})^{-1}D^{f}_{stkl}\right] \tag{8}$$

and S_{ijkl} is the Eshelby tensor [13, 14] of the corresponding reference infinite RVE filled only by bonded elements as depicted in Fig. 4 (b), where the reference RVE has undergone the same eigenstrain increment $\mathrm{d}\varepsilon^{*}_{ij}$ as the frictional-elements RVE and it is entirely identical to the frictional-elements RVE in terms of configuration and elastic property.

It should be noted that both the Eshelby-form tensor S^{ep}_{ijkl} and Eshelby tensor S_{ijkl} do not depend on the given size of the eigenstrain area Ω and the value of the eigenstrain increment $\mathrm{d}\varepsilon^{*}_{ij}$, but only the properties of the filling materials of RVE and the geometry of the eigenstrain area Ω. To simplify, in case of a spherical area Ω, which is an ellipse inclusion with the equal semi-major axis and semi-minor axis, Eshelby tensor S_{ijkl} can be determined with the Green formula and ultimately given as follows:

$$S_{ijkl} = \chi\delta_{ij}\delta_{kl} + \psi\left(\delta_{ik}\delta_{jl} + \delta_{il}\delta_{jk} - \frac{2}{3}\delta_{ij}\delta_{kl}\right) \tag{9}$$

where

$$\chi = \frac{(1+\nu^{re})}{[9(1-\nu^{re})]} \tag{10}$$

$$\psi = \frac{(4-5\nu^{re})}{[15(1-\nu^{re})]} \tag{11}$$

and ν^{re} is denoted by the Poisson ratio of the corresponding reference RVE, which is equal to the Poisson ratio of frictional-elements RVE ν^{fe}. In the Fig. 4 (a), substituting the eigenstrain area Ω with an arbitrary elastic bonded element denoted by Ω^{b} (regarded as inclusion in meso-mechanics), as shown in Fig. 4 (c), it comes to be a single elastic spherical inclusion problem for the relative infinite elastoplastic RVE (regarded as matrix in meso-mechanics). And thus, under a given boundary condition, the Eshelby equivalent inclusion method [13, 14] can be adopted in solution, since the equilibrium condition, boundary condition and consistency condition have not changed. The only alteration in the solution is just to simply replace the elastic modulus with the tangent elastoplastic modulus of frictional elements (matrix materials). And it can be finally expressed with the increment form as follows:

$$D^{f}_{ijkl}\left(d\varepsilon^{frve}_{kl} + \mathrm{d}\varepsilon^{t}_{kl} - \mathrm{d}\varepsilon^{*}_{kl}\right) = D^{b}_{ijkl}\left(d\varepsilon^{frve}_{kl} + \mathrm{d}\varepsilon^{t}_{kl}\right) \tag{12}$$

where $d\varepsilon^{frve}_{ij}$ is the average strain increment of the frictional-elements RVE in Fig. 4 (c), which includes a single bonded element and does not undergo any eigenstrain increments.

Combining Eqs. (7), (8) and (12) gives the following expression:

$$\mathrm{d}\varepsilon_{ij}^{b} = [I_{ijkl} + S_{ijmn}^{ep}(D_{mnop}^{f})^{-1}(D_{opkl}^{b} - D_{opkl}^{f})]^{-1} d\varepsilon_{kl}^{frve} \quad (13)$$

where

$$I_{ijkl} = {}^{1}/_{2}\,(\delta_{ik}\delta_{jl} + \delta_{il}\delta_{jk}) \quad (14)$$

The components of a tailing soils RVE are not constant during the loading process since the bonded elements can gradually break up and transform to frictional elements with the increasing deformation or strain. However, the proportion of frictional elements (matrix materials) and bonded elements (inclusions) are constant at a fixed strain level, and we can further suppose that the bonded elements are distributed in the frictional-elements RVE in a random, as shown in Fig. 4 (d). Considering the interaction between bonded elements during the loading process, the deformation response between frictional and bonded elements can be obtained based on Eq. (13) by using Mori-Tanaka method [26], with the following expressions:

$$\mathrm{d}\varepsilon_{ij}^{b} = A_{ijkl}\mathrm{d}\varepsilon_{kl}^{f} \quad (15)$$

with

$$A_{ijkl} = [I_{ijkl} + S_{ijmn}^{ep}(D_{mnop}^{f})^{-1}(D_{opkl}^{b} - D_{opkl}^{f})]^{-1} \quad (16)$$

where A_{ijkl} is a tensor of local strain coefficient.

2.3 Formulation of binary-medium constitutive model for tailing soils

2.3.1 Constitutive equation

To quantify the degree of the breakage of the RVE, a breakage ratio R_V is introduced with the following expression:

$$R_V = \frac{V^f}{V} = \frac{(V - V^b)}{V} \tag{17}$$

where V, V^f and V^b are the whole volume of the tailing soil RVE, the volume of frictional elements and the volume of bonded elements, respectively. A tailing soil sample contains sufficient RVE, and thus a simple homogenization theory for heterogeneous materials [40] can be used in the mathematical analysis of tailing soils, based on which the macroscopic average stress of the RVE σ_{ij}^{rve} under an arbitrary breakage ratio R_V can be expressed as:

$$\sigma_{ij}^{rve} = \left({}^{1}/_{V}\right) \int \sigma_{ij}^{loc} dV \tag{18}$$

where the superscript loc represents the mesoscopic local stress.

The average stress tensors of bonded elements σ_{ij}^{b} and frictional elements σ_{ij}^{f} are expressed as follows:

$$\sigma_{ij}^{b} = \left({}^{1}/_{V^b}\right) \int \sigma_{ij}^{loc} dV^b \tag{19}$$

$$\sigma_{ij}^{f} = \left({}^{1}/_{V^f}\right) \int \sigma_{ij}^{loc} dV^f \tag{20}$$

From Eq. (18), it gives:

$$\sigma_{ij}^{rve} = \left({}^{1}/_{V}\right) \int \sigma_{ij}^{loc} dV = \left({}^{V^b}/_{V}\right) \sigma_{ij}^{b} + \left({}^{V^f}/_{V}\right) \sigma_{ij}^{f} \tag{21}$$

Similarly, the average strain of the RVE ε_{ij}^{rve} is given by:

$$\varepsilon_{ij}^{rve} = \left({}^{1}/_{V}\right) \int \varepsilon_{ij}^{loc} dV = \left({}^{V^b}/_{V}\right) \varepsilon_{ij}^{b} + \left({}^{V^f}/_{V}\right) \varepsilon_{ij}^{f} \tag{22}$$

where ε_{ij}^{b} and ε_{ij}^{f} are expressed by:

$$\varepsilon_{ij}^{b} = \left({}^{1}/_{V^b}\right) \int \varepsilon_{ij}^{loc} dV^b \tag{23}$$

$$\varepsilon_{ij}^{f} = \left({}^{1}/_{V^f}\right) \int \varepsilon_{ij}^{loc} dV^f \tag{24}$$

Substituting Eq. (17) into Eq. (23) and Eq. (24), respectively, the average stress σ_{ij}^{rve} and average strain ε_{ij}^{rve} of RVE can be written as the following expressions:

$$\sigma_{ij}^{rve0} = (1 - R_V^0)\sigma_{ij}^{b0} + R_V^0 \sigma_{ij}^{f0} \tag{25}$$

$$\varepsilon_{ij}^{rve0} = (1 - R_V^0)\varepsilon_{ij}^{b0} + R_V^0 \varepsilon_{ij}^{f0} \tag{26}$$

where the superscript 0 denotes the current value of variables.

Eq. (25) and Eq. (26) can be given with an incremental expression as follows:

$$d\sigma_{ij}^{rve} = d\sigma_{ij}^{b} + R_V^0(d\sigma_{ij}^{f} - d\sigma_{ij}^{b}) + dR_V\left(\sigma_{ij}^{f0} - \sigma_{ij}^{b0}\right) \tag{27}$$

$$d\varepsilon_{ij}^{rve} = d\varepsilon_{ij}^{b} + R_V^0(d\varepsilon_{ij}^{f} - d\varepsilon_{ij}^{b}) + dR_V\left(\varepsilon_{ij}^{f0} - \varepsilon_{ij}^{b0}\right) \tag{28}$$

where dR_V denotes the increment of the breakage ratio.

Substituting Eq. (1) and Eq. (3) into Eq. (27) gives

$$d\sigma_{ij}^{rve} = D_{ijkl}^{b} d\varepsilon_{kl}^{b} + R_V^0\left(D_{ijkl}^{f} d\varepsilon_{kl}^{f} - D_{ijkl}^{b} d\varepsilon_{kl}^{b}\right) + dR_V\left(\sigma_{ij}^{f0} - \sigma_{ij}^{b0}\right) \tag{29}$$

Eq. (28) gives

$$d\varepsilon_{ij}^{f} = \frac{1}{R_V^0}\left[d\varepsilon_{ij}^{rve} - d\varepsilon_{ij}^{b} - dR_V\left(\varepsilon_{ij}^{f0} - \varepsilon_{ij}^{b0}\right)\right] + d\varepsilon_{ij}^{b} \tag{30}$$

Combining Eqs. (29) and (30) gives the following expression:

$$d\sigma_{ij}^{rve} = D_{ijkl}^{f} d\varepsilon_{kl}^{rve} - (1 - R_V^0)\left(D_{ijkl}^{f} - D_{ijkl}^{b}\right) d\varepsilon_{kl}^{b} - dR_V D_{ijkl}^{f}\left(\varepsilon_{kl}^{f0} - \varepsilon_{kl}^{b0}\right) + dR_V\left(\sigma_{ij}^{f0} - \sigma_{ij}^{b0}\right) \tag{31}$$

Let $R_V = R_V\left(\varepsilon_{ij}^{rve}\right)$, the increment of R_V can be expressed as follows:

$$dR_V = \left\{\frac{\partial R_V}{\partial \varepsilon_{kl}^{rve}}\right\}^{\mathrm{T}} d\varepsilon_{kl}^{rve} \tag{32}$$

Combing Eqs. (15) and (30), the average strain increment of bonded elements $d\varepsilon_{ij}^{b}$ can be expressed by:

$$d\varepsilon_{ij}^{b} = L_{ijmn}\left[I_{mnkl} - \frac{1}{R_V^0}\left(\varepsilon_{mn}^{rve0} - \varepsilon_{mn}^{b0}\right)\left\{\frac{\partial R_V}{\partial \varepsilon_{kl}^{rve}}\right\}^{\mathrm{T}}\right] d\varepsilon_{kl}^{rve} \tag{33}$$

where L_{ijkl} is defined as the coefficient tensor with the following expression:

$$L_{ijkl} = A_{ijmn}\left[R_V^0 I_{mnkl} + (1 - R_V^0) A_{mnkl}\right]^{-1} \tag{34}$$

Substituting Eq. (33) into Eq. (31) gives

$$d\sigma_{ij}^{rve} = D_{ijkl}^{f} d\varepsilon_{kl}^{rve} - (1 - R_V^0)\left(D_{ijmn}^{f} - D_{ijmn}^{b}\right) L_{mnop}\left[I_{opkl} - \frac{1}{R_V^0}\left(\varepsilon_{op}^{rve0} - \varepsilon_{op}^{b0}\right)\left\{\frac{\partial R_V}{\partial \varepsilon_{kl}^{rve}}\right\}^{\mathrm{T}}\right] d\varepsilon_{kl}^{rve}$$

$$-\left[D_{ijmn}^{f}\left(\varepsilon_{mn}^{f0}-\varepsilon_{mn}^{b0}\right)-\left(\sigma_{ij}^{f0}-\sigma_{ij}^{b0}\right)\right]\left\{\frac{\partial R_V}{\partial \varepsilon_{kl}^{rve}}\right\}^{\mathrm{T}} d\varepsilon_{kl}^{rve} \tag{35}$$

Eqs. (25) and (26) give

$$\sigma_{ij}^{f0}-\sigma_{ij}^{b0}=\frac{1}{R_V^0}\left(\sigma_{ij}^{rve0}-\sigma_{ij}^{b0}\right) \tag{36}$$

$$\varepsilon_{ij}^{f0}-\varepsilon_{ij}^{b0}=\frac{1}{R_V^0}\left(\varepsilon_{ij}^{rve0}-\varepsilon_{ij}^{b0}\right) \tag{37}$$

Combining Eqs. (1), (35), (36) and (37), the constitutive relations of tailing soils can be given as follows:

$$\begin{aligned} d\sigma_{ij}^{rve} &= D_{ijkl}^{f} d\varepsilon_{kl}^{rve}-\left(1-R_V^0\right)\left(D_{ijmn}^{f}-D_{ijmn}^{b}\right)L_{mnop}\, d\varepsilon_{op}^{rve} \\ &\quad +\frac{1}{R_V^0}\left\{\left[\left(1-R_V^0\right)\left(D_{ijmn}^{f}-D_{ijmn}^{b}\right)L_{mnop}-D_{ijop}^{f}\right]\left(\varepsilon_{op}^{rve0}-\varepsilon_{op}^{b0}\right)\right. \\ &\quad \left.+\left(\sigma_{ij}^{rve0}-D_{ijmn}^{b}\varepsilon_{mn}^{b0}\right)\right\}\left\{\frac{\partial R_V}{\partial \varepsilon_{kl}^{rve}}\right\}^{\mathrm{T}} d\varepsilon_{kl}^{rve} \end{aligned} \tag{38}$$

Eq. (38) indicates that the average stress increment of RVE can be decomposed into three components, in which the first portion denotes the stress increment when the RVE is considered to be entirely composed of frictional elements, and the second portion shows that the existence of bonded elements contributes to the decrease of stress increment, with the final component presenting the impact of the breakage.

During the frozen process at the open environment, the continued growth of the ice-crystal network increases the pore size and the volume of tailing soil samples, part of adsorbed water, unstable compound and cement failure due to nonuniform distribution of stress and strain inside RVE. Thus, the bonded elements selected previously may lose their high cohesive force. However, based on meso-mechanics, the coefficient tensor L_{ijkl}, which connects the average strain of bonded elements and average strain of RVE, do not be affected by the size of bonded elements (or frictional elements), and thus a bigger spherical area contains adsorbed water, unstable compound and cement can be selected as bonded element for tailing soils exposed to freeze-thaw cycles. In addition, in the following thawing process, the plastic deformation does not get back to the original state, leading to a strength deterioration of tailing soils. In the proposed constitutive model, the effects of freeze-thaw cycles on meso-structure of tailing soils can be described as the decrease in modulus and variation in parameters of the bonded and frictional elements.

In the following sections, the stress and strain invariants are employed in the formulation, with the mean stress σ_m and generalized shear stress σ_s are respectively denoted by:

$$\sigma_m = \frac{1}{3}\sigma_{kk} \tag{39}$$

$$\sigma_s = \sqrt{\frac{3}{2}s_{ij}s_{ij}}, s_{ij} = \sigma_{ij} - \sigma_{kk}\delta_{ij} \tag{40}$$

Similarly, the volumetric strain ε_v and distortional strain ε_s are respectively expressed as:

$$\varepsilon_v = \varepsilon_{kk} \tag{41}$$

$$\varepsilon_s = \sqrt{\frac{3}{2}e_{ij}e_{ij}}, e_{ij} = \varepsilon_{ij} - \frac{1}{3}\varepsilon_{kk}\delta_{ij} \tag{42}$$

Therefore, those above four-order tensors $D_{ijkl}^{b}, D_{ijkl}^{fe}, D_{ijkl}^{f}, S_{ijkl}, S_{ijkl}^{ep}, A_{ijkl}, L_{ijkl}$, and I_{ijkl} can be written in the form of 2 × 2 matrix as $[D_{xy}^{b}], [D_{xy}^{fe}], [D_{xy}^{f}], [S_{xy}], [S_{xy}^{ep}], [A_{xy}], [L_{xy}], [I_{xy}]$, where the subscripts $x = m, \mathrm{s}$ and $y = v, \mathrm{s}$ and the summation convention does not operate here.

And then, the constitutive relations of tailing soils [Eq. (38)] can be also rewritten as

$$\begin{Bmatrix} d\sigma_m^{rve} \\ d\sigma_s^{rve} \end{Bmatrix} = [B_{xy}] \begin{Bmatrix} d\varepsilon_v^{rve} \\ d\varepsilon_s^{rve} \end{Bmatrix} \tag{43}$$

where

$$\begin{aligned} [B_{xy}] &= [D_{xy}^{f}] - (1 - R_V^0)\left[[D_{xy}^{f}] - [D_{xy}^{b}]\right][L_{xy}] \\ &\quad + \frac{1}{R_V^0}\left\{\left((1 - R_V^0)\left([D_{xy}^{f}] - [D_{xy}^{b}]\right)[L_{xy}] - [D_{xy}^{f}]\right)\left(\begin{Bmatrix} \varepsilon_v^{rve0} \\ \varepsilon_s^{rve0} \end{Bmatrix} - \begin{Bmatrix} \varepsilon_v^{b0} \\ \varepsilon_s^{b0} \end{Bmatrix}\right)\right. \\ &\quad \left. + \left(\begin{Bmatrix} \sigma_m^{rve0} \\ \sigma_s^{rve0} \end{Bmatrix} - [D_{xy}^{b}]\begin{Bmatrix} \varepsilon_v^{b0} \\ \varepsilon_s^{b0} \end{Bmatrix}\right)\right\}\begin{Bmatrix} \partial R_V / \partial \varepsilon_v^{rve} \\ \partial R_V / \partial \varepsilon_s^{rve} \end{Bmatrix}^{\mathrm{T}} \end{aligned} \tag{44}$$

As presented in Eq. (43) and Eq. (44), the current model has four sets of parameters, including the strain coefficient, the breakage parameter and the constitutive parameters of bonded elements and frictional elements. These model parameters can be evaluated by triaxial compression tests with an assumption function of the particle breakage.

2.3.2 Constitutive relationship of bonded elements

The bonded element is a spherical collection of tailing soil skeleton, which is occupied with crystal water, unstable compounds, and cement, with strong cohesive resistance. The bonded elements here are assumed to be homogeneous, isotropic and incrementally linearized, and its stress-strain relationship [Eq. (1)] is assumed to obey the generalized Hooke's law as the following expression:

$$\begin{Bmatrix} d\sigma_m^b \\ d\sigma_s^b \end{Bmatrix} = \begin{bmatrix} D_{mv}^b & D_{ms}^b \\ D_{sv}^b & D_{ss}^b \end{bmatrix} \begin{Bmatrix} d\varepsilon_v^b \\ d\varepsilon_s^b \end{Bmatrix} = \begin{bmatrix} K^b & 0 \\ 0 & 3G^b \end{bmatrix} \begin{Bmatrix} d\varepsilon_v^b \\ d\varepsilon_s^b \end{Bmatrix} \tag{45}$$

where K^b and G^b are the elastic bulk modulus and shear modulus of bonded elements, respectively. At the initial loading within a very small strain range, the bonded elements are hardly broken, they occupy the whole volume of tailing soils RVE. Therefore, the elastic bulk modulus K^b and shear modulus G^b of bonded elements can be determined by the tailing soil samples at the initial loading stage.

2.3.3 Constitutive relationship of frictional elements

The frictional element is a spherical area that originates from the bonded element when whose brittle bonds have been completely broken, hence the mechanical properties of frictional elements can be assumed to be the same as those of the remolded tailing soils samples, which are reconstituted by using the particles of the tailing soil samples that have been experienced triaxial compression experiments. Here, a double hardening model [21, 35] for saturated soils is introduced and modified to cater for the elastoplastic behavior of frictional elements. The parameters of the double hardening model are given based on the test results of the triaxial compression tests.

According to classical plasticity, the average strain incremental of frictional elements [Eq. (6)] can be given:

$$\begin{Bmatrix} d\varepsilon_v^f \\ d\varepsilon_s^f \end{Bmatrix} = \begin{Bmatrix} d\varepsilon_v^{fe} \\ d\varepsilon_s^{fe} \end{Bmatrix} + \begin{Bmatrix} d\varepsilon_v^{fp} \\ d\varepsilon_s^{fp} \end{Bmatrix} \tag{46}$$

Based on double hardening model introduced, the elastic strain can be obtained by the generalized Hooke's law as following:

$$\begin{Bmatrix} d\varepsilon_v^{fe} \\ d\varepsilon_s^{fe} \end{Bmatrix} = \begin{bmatrix} D_{mv}^{fe} & D_{ms}^{fe} \\ D_{sv}^{fe} & D_{ss}^{fe} \end{bmatrix}^{-1} \begin{Bmatrix} d\sigma_m^f \\ d\sigma_s^f \end{Bmatrix} = \begin{bmatrix} K^{fe} & 0 \\ 0 & 3G^{fe} \end{bmatrix}^{-1} \begin{Bmatrix} d\sigma_m^f \\ d\sigma_s^f \end{Bmatrix} \tag{47}$$

where K^{fe} and G^{fe} are the elastic bulk modulus and elastic shear modulus of the frictional elements, respectively, which can be determined by triaxial compression tests.

The yielding function of the double hardening model is expressed as:

$$\phi = \frac{\sigma_m^f}{1 - [\frac{\eta}{\Gamma_\phi}]^n} - \Theta \tag{48}$$

and

$$\eta = \frac{\sigma_s^f}{\sigma_m^f} \tag{49}$$

where n is a power number varying with the confining pressures; and Γ_ϕ and Θ are two hardening parameters which are the functions of plastic volumetric strain ε_v^{fp} and plastic shear strain ε_s^{fp}, with the following expressions, respectively:

$$\Theta = \Theta(\varepsilon_v^{fp}) = p_0 exp\left(\frac{\varepsilon_v^{fp}}{c_c - c_d}\right) \tag{50}$$

$$\Gamma_\phi = \Gamma_\phi(\varepsilon_s^{fp}) = \alpha_\phi - (\alpha_\phi - \alpha_{\phi 0}) exp(\varepsilon_s^{fp}) \tag{51}$$

where p_0 denotes the reference stress, and c_c, c_d, α_ϕ and $\alpha_{\phi 0}$ are material parameters obtained by triaxial compression tests. Fig. 5 shows a schematic diagram of the yield surface on the deviatoric stress q-mean stress p plane. The model is an isotropic hardening model and the yield surface both expands and contracts with the variation of hardening parameters. Besides, the proportion variation of two hardening parameters can change the shape of the yield surface, extending the applicability of the model for complicated stress path.

Taking the non-associated flow rule into account, the plastic potential function is assumed to be similar to the yielding function, with the following expression:

$$g = \frac{\sigma_m^f}{1 - [\frac{\eta}{\Gamma_g}]^w} - \Theta \tag{52}$$

where w is a model parameter varying with the confining pressures, and Γ_g is a hardening parameter expressed as follows:

$$\Gamma_g = \Gamma_g\left(\varepsilon_s^{fp}\right) = \alpha_g - \left(\alpha_g - \alpha_{g0}\right)\exp\left(\varepsilon_s^{fp}\right) \tag{53}$$

with α_g and α_{g0} are material parameters obtained by triaxial compression tests. If selecting $\alpha_{\phi 0} = \alpha_\phi$ and $\alpha_{g0} = \alpha_g$, the double hardening model can degenerate to the conventional elastoplastic model with a single hardening parameter. As shown in Fig. 5, the yield surface and potential surface passing the same plastic strain point have different exterior normal line.

Hence, according to the classical plasticity, the stress-strain relationship [Eq. (3)] of the frictional elements can be expressed as follow:

$$\begin{aligned}
\begin{Bmatrix} d\sigma_m^f \\ d\sigma_s^f \end{Bmatrix} &= \begin{bmatrix} D_{mv}^f & D_{ms}^f \\ D_{sv}^f & D_{ss}^f \end{bmatrix} \begin{Bmatrix} d\varepsilon_v^f \\ d\varepsilon_s^{f)} \end{Bmatrix} \\
&= \left[\begin{bmatrix} K^{fe} & 0 \\ 0 & 3G^{fe} \end{bmatrix} - \frac{\begin{bmatrix} K^{fe} & 0 \\ 0 & 3G^{fe} \end{bmatrix} \begin{Bmatrix} \frac{\partial g}{\partial \sigma} \end{Bmatrix} \begin{Bmatrix} \frac{\partial \phi}{\partial \sigma} \end{Bmatrix}^T \begin{bmatrix} K^{fe} & 0 \\ 0 & 3G^{fe} \end{bmatrix}}{H + \begin{Bmatrix} \frac{\partial \phi}{\partial \sigma} \end{Bmatrix}^T \begin{bmatrix} K^{fe} & 0 \\ 0 & 3G^{fe} \end{bmatrix} \begin{Bmatrix} \frac{\partial g}{\partial \sigma} \end{Bmatrix}} \right] \begin{Bmatrix} d\varepsilon_v^f \\ d\varepsilon_s^f \end{Bmatrix}
\end{aligned} \tag{54}$$

where H denotes Hardening modulus, which can be calculated as

$$\begin{aligned}
H &= -\frac{\partial \phi}{\partial \Gamma_\phi} \frac{\partial \Gamma_\phi}{\partial \varepsilon_s^{fp}} \frac{\partial g}{\partial \sigma_s^f} - \frac{\partial \phi}{\partial \Theta} \frac{\partial \Theta}{\partial \varepsilon_v^{fp}} \frac{\partial g}{\partial \sigma_m^f} \\
&= -\left[\frac{n \sigma_m^f \eta^n \left(\alpha_\phi - \Gamma_\phi\right)}{{\Gamma_\phi}^{(n+1)} \left[1 - \left(\eta / \Gamma_\phi\right)^n\right]^2} \right] \left[\frac{w \eta^{(w-1)}}{{\Gamma_g}^w \left[1 - \left(\eta / \Gamma_g\right)^w\right]^2} \right]
\end{aligned}$$

$$-\frac{\Theta}{c_c - c_s}\left[\frac{w\eta^w}{{\Gamma_g}^w\left[1-\left(\eta/\Gamma_g\right)^w\right]^2} - \frac{1}{1-\left(\eta/\Gamma_g\right)^w}\right] \quad (55)$$

2.3.4 The breakage ratio

The breakage ratio R_V is regarded as an internal variable, which is a structure parameter depending on soil type, stress and strain level, loading history and stress path. It should be determined by performing an analysis on meso-structure and meso-mechanic properties of the materials. However, it’s hard to give a dynamic evolution of the breakage with reliable accuracy based on the current experimental apparatus. Therefore, the evolving relationship of breakage ratio is established using similar determination methods of hardening parameters in plasticity or damage factors in damage mechanics. Theoretically, the evolution of breakage ratio R_V should be consistent with the following rules: $R_V \to 0$ at the initial loading, referring to that the bonded elements are hardly broken; $R_V \to 1$ at the high strain level, which means the bonded elements are almost entirely broken; and R_V increases from 0 to 1 with increasing deformation or strain level, accompanied with the bonded elements gradually break up and transform to be frictional elements. In the view of meso-mechanism, the brittle bonds of the bonded elements seem to be broken due to the increasing tension strain and hardly be affected by the spherical strain. However, tailing soils are porous mediums, besides face-corner contact, face-face contact also exists between particles. Hence the brittle bonds can also be broken when experienced increasing spherical strain, and thus, the breakage ratio R_V is assumed to be a function of generalized shear strain and volumetric strain of RVE, with the following expression:

$$R_V = 1 - \exp\left[-\beta\left|\varepsilon_v^{rve}\right|^{\psi} - \zeta\left|\varepsilon_s^{rve}\right|^{\varpi}\right] \quad (56)$$

where $|x|$ is the absolute value of variable x; β, ζ and ϖ are material parameters varying with confining pressures; and ψ is material constant. The evolution of parameters β, ζ and ϖ is given by fitting with the triaxial test data of tailing soil samples. Fig. 6 (a) shows that at the initial loading stage, the breakage ratio R_V almost presents a linear increase at various value of β, which is responsible for the fissures generating inside brittle bonds. Therefore, a subsequent slight disturbance can aggravate the breakage process of bonded elements. Then, the breakage ratio gradually increases and finally reaches an extremum value of 1, at this stage of which tailing soil sample entirely consists of frictional elements. The evolution rules of the breakage ratio R_V under different material parameters, shown in Fig. 6 (b) and (c), are similar to that of Fig. 6 (a).

2.3.5 The strain coefficient tensor

By employing a strain coefficient tensor L_{ijkl}, the strain relationship between the bonded elements and RVE under an arbitrary breakage ratio R_V are given in Eq. (33), which can also be could be expressed with stress and strain invariants as follows:

$$\begin{Bmatrix} d\varepsilon_v^b \\ d\varepsilon_s^b \end{Bmatrix} = \begin{bmatrix} L_{mv} & L_{ms} \\ L_{sv} & L_{ss} \end{bmatrix} \left\{ \begin{bmatrix} I_{mv} & I_{ms} \\ I_{sv} & I_{ss} \end{bmatrix} - \frac{1}{R_V^0} \left\{ \begin{Bmatrix} \varepsilon_v^{rve0} \\ \varepsilon_s^{rve0} \end{Bmatrix} - \begin{Bmatrix} \varepsilon_v^{b0} \\ \varepsilon_s^{b0} \end{Bmatrix} \right\} \begin{Bmatrix} \partial R_V / \partial \varepsilon_v^{rve} \\ \partial R_V / \partial \varepsilon_s^{rve} \end{Bmatrix}^{\mathrm{T}} \right\} \begin{Bmatrix} d\varepsilon_v^{rve} \\ d\varepsilon_s^{rve} \end{Bmatrix} \quad (57)$$

The elements of matrix $[L_{ij}]$ can be determined through the given constitutive relationships of bonded elements and frictional elements, with the following expressions:

$$\begin{bmatrix} L_{mv} & L_{ms} \\ L_{sv} & L_{ss} \end{bmatrix} = \begin{bmatrix} A_{mv} & A_{ms} \\ A_{sv} & A_{ss} \end{bmatrix} \left[R_V^0 \begin{bmatrix} I_{mv} & I_{ms} \\ I_{sv} & I_{ss} \end{bmatrix} + (1 - R_V^0) \begin{bmatrix} A_{mv} & A_{ms} \\ A_{sv} & A_{ss} \end{bmatrix} \right]^{-1} \quad (58)$$

$$\begin{bmatrix} A_{mv} & A_{ms} \\ A_{sv} & A_{ss} \end{bmatrix} = \left[\begin{bmatrix} I_{mv} & I_{ms} \\ I_{sv} & I_{ss} \end{bmatrix} + \begin{bmatrix} S_{mv}^{ep} & S_{ms}^{ep} \\ S_{sv}^{ep} & S_{ss}^{ep} \end{bmatrix} \begin{bmatrix} D_{mv}^f & K_{ms}^f \\ D_{sv}^f & K_{ss}^f \end{bmatrix}^{-1} \left(\begin{bmatrix} D_{mv}^b & D_{ms}^b \\ D_{sv}^b & D_{ss}^b \end{bmatrix} - \begin{bmatrix} D_{mv}^f & D_{ms}^f \\ D_{sv}^f & D_{ss}^f \end{bmatrix} \right) \right]^{-1} \quad (59)$$

$$\begin{bmatrix} S_{mv}^{ep} & S_{ms}^{ep} \\ S_{sv}^{ep} & S_{ss}^{ep} \end{bmatrix} = \left\{ \begin{bmatrix} D_{mv}^f & D_{ms}^f \\ D_{sv}^f & D_{ss}^f \end{bmatrix}^{-1} \begin{bmatrix} D_{mv}^b & D_{ms}^b \\ D_{sv}^b & D_{ss}^b \end{bmatrix} \right\}^{-1} \begin{bmatrix} S_{mv} & S_{ms} \\ S_{sv} & S_{ss} \end{bmatrix} \left\{ \begin{bmatrix} D_{mv}^f & D_{ms}^f \\ D_{sv}^f & D_{ss}^f \end{bmatrix}^{-1} \begin{bmatrix} D_{mv}^b & D_{ms}^b \\ D_{sv}^b & D_{ss}^b \end{bmatrix} \right\} \quad (60)$$

3. Model calibration and evaluation

In this section, the determination of model parameters is presented. For calibrating and evaluation of the proposed model, the previous experimental data [24] of drained compression triaxial tests of saturated zinc tailing soils are employed, the tailing soil used was extracted from a seasonally frozen region. In the experiments, a series cylinder specimens which were 39.1 mm in diameter and 80 mm in height were prepared. The samples were saturated by vacuum and hydraulic method until the pore pressure parameter B reached beyond 0.95, and the freeze-thaw process was conducted in an open environment with no confining pressure applying, meanly, water exchange with surroundings was allowed during freeze-thaw process. A freeze-thaw process lasted for 24h and the tested freezing and thawing temperatures range from -20℃ to 40℃ with the number of freeze-thaw cycles N=0, 1, 5 and 15. Besides, the specimens with N=0 were pulverized and remodeled after they have been subjected to triaxial tests, and the newly generated frictional samples, which are entirely composed of frictional elements, were employed to determine the parameters of frictional elements.

In an open environment, the samples are kept at a saturated state, the samples experienced increased volume and weight after freeze-thaw cycles. The volume and weight variation of tailing soil samples after freeze-thaw cycles were recorded in the experiments, as their average weight-growth ratio shown in Fig. 7 (a), which is defined as a ratio between the sample’s weight increment after freeze-thaw cycles and its initial weight. The increased weight of the tailing soil sample majorly results from the water supplement, which is a consistent tendency with the volume increment of the specimen, as shown in Fig. 7 (b). Therefore, the decrease in density and increase in pore size are important factors that decrease the strength of tailing soils. However, the volume change majorly occurs in the axial direction due to the restraining effect of rubber mold during freeze-thaw process. After 15 numbers of freeze-thaw cycles, the volume of tailing specimens dilated by 22.03% with a 7.2 mm increase in height but only with a 2.3 mm growth in diameter, therefore, the pervious stones which diameter is a bit larger than 39.1mm was applied during the triaxial test.

Under triaxial stress conditions, the maximal principal stress is applied along the vertical direction, which is set as the z-axial direction, and thus, the stress and strain invariants can be simplified as the follows:

$$\sigma_m = (\sigma_1 + 2\sigma_3)/3 \tag{61}$$

$$\sigma_s = \sigma_1 - \sigma_3 \tag{62}$$

$$\varepsilon_v = \varepsilon_1 + 2\varepsilon_3 \tag{63}$$

$$\varepsilon_s = 2(\varepsilon_1 - \varepsilon_3)/3 \tag{64}$$

3.1 Parameter determination for bonded elements

Tailing soils specimens at the initial loading stage are regarded as materials entirely composed of bonded elements, and hence the mechanical properties of bonded elements are regarded to be the same as those of tailing soil specimens at this stage. Under triaxial conditions, a distortional strain ε_s of 0.4% is adopted to calculate the elastic bulk modulus K^b and shear modulus G^b of tailing soil samples based on the previous experimental data, with the results presented in Fig. 8. At a various number of freeze-thaw cycles N, both elastic bulk modulus K^b and shear modulus G^b can be fitted with exponential functions, with expressed as $K^b = X_1(-N/t_1) + Y_1$ and $G^b = X_2(-N/t_2) + Y_2$, respectively. And under the confining pressure σ_3= 50kPa, 100kPa, 200kPa and 300kPa, the fitting parameters are taken as $X_1 =$ 22912.80, 22004.05, 18725.92 and 17973.74, t_1 =1.35, 1.31, 1.24 and 1.19, $Y_1 =$ 4090.77, 5449.33, 9424.85 and 11092.08, $X_2 =$ 17556.45, 17434.15, 17261.43 and 16681.79, $t_2 =$ 0.90, 1.74, 1.78 and 1.85, and $Y_2 =$ 3545.62, 4615.12, 12204.60 and 15793.85, respectively.

3.2 Parameter determination for frictional element

After triaxial compression tests, the bonded elements are entirely broken, and they all transform into frictional elements. By pulverizing and remodeling the tailing soil samples after they have been subjected to triaxial tests, new triaxial specimens entirely composed of frictional elements can be obtained, which obtained through this method are called frictional samples.

The mechanical properties of frictional elements are assumed to be the same as those of the frictional samples, therefore, the parameters of frictional elements here are determined with the previous results of the frictional tailing soils samples, which are presented in Fig. 9. The elastic bulk modulus K^{fe} and shear modulus G^{fe} of frictional elements are obtained based on a distortional strain ε_s =0.4%. Besides, Eq. (50) has a similar form as the equation in Cam-caly model, where p_0 is the reference confining pressures at $\varepsilon_v^{fp} = 0$ in drained triaxial compression tests. The parameter c_c is determined by $c_c = \lambda/(1+e_0)$, where λ denotes the virgin compression slope on $\varepsilon_v^f - \ln p^f$ plot in the isotropic compression tests, and e_0 denotes the initial void ratio. The parameter c_d can be expressed by $c_d = M[\kappa/(1+e_0)]\exp(-Z\,\sigma_3/P_a)$, where κ is the rebounding slope on $\varepsilon_v^f - \ln p^f$ plot, and the parameters M and Z are material constants, with the parameter P_a denoting the standard atmospheric pressure, which is approximately equal to 101.4kPa. In Eq. (51), $\alpha_\phi = \sqrt[n]{1+n sin\varphi_r}$, where φ_r denotes the residual angle of inner friction, and $n = -a_1\ln(\sigma_3) + b_1$; $\alpha_{\phi 0}$ reflects the contribution degree of the generalized shear strain, and it is determined by $\alpha_{\phi 0} = \Lambda_\phi \alpha_\phi$, where Λ_ϕ is a material constant with $0 \le \Lambda_\phi \le 1$. In Eq. (53), $\alpha_g = \sqrt[w]{1+\mathrm{w} sin\varphi_r}$ and $\alpha_{g0} = \Lambda_g \alpha_g$, where Λ_g is another material constant with $0 \leq \Lambda_g \leq 1$, $w = -a_2 \ln(\sigma_3) + b_2$. a_1, a_2, b_1, and b_2 are material parameters.

Under the number of freeze-thaw cycles $N = 0$, at confining pressure σ_3 =50kPa, 100kPa, 200kPa and 300kPa, the elastic bulk modulus $K^{fe} =$ 33243kPa, 32624kPa, 33869kPa and 33981kPa and shear modulus $G^{fe} =$ 9303, 12373, 13704, and 18417 kPa, respectively. Other experimental parameters of frictional elements under $N = 0$ are obtained from the test results of triaxial tests of the frictional tailing soil samples: virgin compression slope $\lambda = 0.123$, rebounding slope $\kappa = 0.025$, initial void ratio $e_0 =$ 1.1, residual angle of inner friction $\varphi_r = 32^0$.

The experimental parameters of the frictional tailing soil samples under $N =$ 1, 5 and 15 are determined based on those under *N*=0. Similar to the determination of the elastic bulk modulus K^b and shear modulus G^b for bonded elements, the elastic bulk modulus K^{fe} and shear modulus G^{fe} of frictional samples under a different number of freeze-thaw cycles are fitted by: $K^{fe} = X_3(-N/t_3) + Y_3$ and $G^{fe} = X_4(-N/t_4) + Y_4$, respectively. And under the confining pressure σ_3= 50kPa, 100kPa, 200kPa and 300kPa, the fitting parameters are taken as $X_3 =$ 29626.89, 28419.62, 27799.90 and 27527.19, $t_3 =$ 1.14, 1.40, 1.86 and 2.07, $Y_3 =$ 3615.80, 4203.98, 6068.90 and 6454.12, $X_4 =$ 8150.17, 9754.30, 10224.40 and 12893.71, $t_4 =$ 1.28, 1.58, 2.59 and 2.85, and $Y_4 =$ 1152.60, 2618.87, 3479.30 and 5523.45, respectively. Besides, experimental parameters of the frictional tailing soils samples λ, κ, φ_r and e_0 under various number of freeze-thaw cycles are given by: $\lambda = -0.010exp(-N/-0.139) + 0.136$, $\kappa = 0.012\exp(-N/1.692) + 0.013$, $\varphi_r = 7.95(-N/2.19) + 23.63$ and $e_0 = -0.29(-N/2.76) + 1.39$. In addition, under the confining pressure of 50kPa, 100kPa, 200kPa and 300kPa, material parameters $M = 4.263$, 45.62, 8.49, 48.83, $Z = 0.06$, 0.21, 0.39, 0.82, $a_1 = -1.13$, -0.88, -0.54, -0.84, $a_2 = 3.62$, 3.60, 3.54, 3.47, and $b_1 = 8.4$, 7.2, 5.5, 5.0, respectively. Finally, the rest of material constants have a fixed value at an arbitrary number of freeze-thaw cycles and confining pressures: $b_2 = 0.002$, $\Lambda_\phi = 0.8$, and $\Lambda_g = 0.72$.

3.3 Parameter determination for the breakage ratio

In this paper, the breakage ratio R_V for tailing soils is regarded as an internal variable, whose dominant parameters are very difficult to establish at meso-scale based on the existing testing technology. It is considered that the compaction effect on tailing soils can be enhanced as the increasing confining pressures, which will improve the stiffness of brittle bond and slow down the ratio of bond breaking, even though a slight breakage may happen at the consolidation procedure. Therefore, the impact of confining pressure is implicitly integrated into the breakage ratio R_V, with the material parameters β, ζ and ϖ expressed by: $\beta = \beta_0 {\sigma_3}^{\gamma}$, $\zeta = \zeta_0 \sigma_3 + o$, and $\varpi = \varpi_0 \ln(\sigma_3) + \theta$, where β_0, γ and o are model parameters, and ζ_0, ϖ and θ are material constants. ϕ_0 takes a constant value with various confining pressures.

Here, the above parameters can be obtained by fitting with the test results. Under the number of freeze-thaw cycles $N = 0,\ 1,\ 5$ and 15, the model parameters $\beta_0 = 0.074,\ 0.103,\ 0.105,\ 0.180$, $\gamma = 0.54,\ 0.52,\ 0.45,\ 0.44$, $o = 45,\ 25,\ 15,\ 4$, and $\psi_0 = 0.030,\ 0.037,\ 0.048$ and 0.050, respectively. Besides, material constants $\zeta_0 = 0.03$, $\varpi_0 = -0.213$, and $\theta = 1.5$ for various confining pressures and an arbitrary number of freeze-thaw cycles.

3.4 Parameter determination for the strain coefficient tensor

For the spherical bonded elements, the matrix form of the Eshelby tensor S^e_{ijkl} under triaxial compression conditions can be determined by:

$$\left[S_{xy}\right] = \begin{bmatrix} S_{mv} & S_{ms} \\ S_{sv} & S_{ss} \end{bmatrix} = \begin{bmatrix} 3K^{s} & 0 \\ 0 & 2G^{s} \end{bmatrix} \tag{65}$$

$$K^{s} = \frac{1+\nu^{fe}}{9(1-\nu^{fe})};\ G^{s} = \frac{4-5\nu^{fe}}{15(1-\nu^{fe})} \tag{66}$$

where ν^{fe} is the elastic Poisson ratio of the frictional elements, which can be determined from the elastic bulk modulus and elastic shear modulus of the frictional elements. And matrix $\left[I_{xy}\right]$ gives

$$\begin{bmatrix} I_{mv} & I_{ms} \\ I_{sv} & I_{ss} \end{bmatrix} = \begin{bmatrix} 1/3 & 0 \\ 0 & 3/2 \end{bmatrix} \tag{67}$$

And thus, the strain coefficient tensor L_{ijkl} under triaxial compression conditions can be obtained by Eq. (58) incorporated with the breakage ratio and the constitutive relationships of bonded elements and frictional elements obtained previously.

3.5 Model Verification

To further confirm the reasonability and applicability of the model proposed here, the comparisons between the computed results with the previous tested data are depicted in Fig. 10, where T-x kPa and C-x kPa represent the tested and computed results at a confining pressure of x kPa, respectively. Comparisons with the previous experimental date demonstrate that under low confining pressures within a small number of freeze-thaw cycles (N=0-σ_3=50kPa, N=0-σ_3=100kPa and N=1-σ_3=50kPa), the proposed model can describe the strain-softening behavior of tailing soils, which is accompanied by a volume contraction followed by volume dilation behavior. Although the computed peak deviatoric stresses present a slight delay than those of the experimental results, their residual strength is very close.

Besides, the other computed results agree well with the tested results. As presented in the figure that the computed results with relative lager number of freeze-thaw cycles under low confining pressures (N=1-σ_3=100kPa, N=5-σ_3=50kPa and N=5-σ_3=100kPa) present strain-softening behavior and volume compression. In addition, the rest of the computed results all present strain-hardening behavior with the volume contracting all the time.

Although there are slight differences in values between the computed and tested results, the results demonstrate that the theoretical model proposed can reproduce the major aspects of the freeze-thaw influences on the mechanical behaviors of tailing soils, and the predicted results are in well agreement with the tested data.

4. Conclusions

In this study, a new binary-medium constitutive has been developed for freeze-thaw tailing soils based on the homogenization theory. The new constitutive model proposed here idealizes the tailing soils as composite materials composed of bonded elements and frictional elements, which are described by generalized Hooke's law and a double hardening model, respectively, and the failure or breakage mechanism of tailing soils is discussed at a multi-scale coupling of macroscopic and mesoscopic views. Compared with the previous binary-medium constitutive, the strain coefficient tensor connecting the strain of bonded elements with the strain of RVE has been derived based on meso-mechanics and the breakage mechanism. The comparisons between the computed and experimental results demonstrate that the new theoretical model can reproduce the main influence of the freeze-thaw cycles on the mechanical behavior of tailing soils, including the strain-softening behavior and the volume contraction behavior followed by a volume dilatancy under low confining pressures within a small number of freeze-thaw cycles, and the slight strain-softening behavior with a continuous volume contraction behavior under low confining pressures with a relative lager number of freeze-thaw cycles, as well as the strain-hardening behavior accompanied by a continuous volume contraction under high confining pressure and large number of freeze-thaw.

Acknowledgements

The authors appreciate the reviewers and Editor very much for their comments. This research was supported by National Science Foundation of China (Grant No. 41790431).

Nomenclature

superscript b denotes the variable of bonded elements

superscript f denotes the variable of frictional elements

superscript frve denotes the variable of frictional − elements RVE

superscript rve denotes the variable of representative volume element (RVE)

superscript *loc* denotes the ssmesoscopic local variable

superscript 0 denotes the current value of variables

ε_{ij} *stress tensor*

ε_{ij} *stain tensor*

ε_{ij}^{*} *eigenstrain tensor*

ε_{ij}^{t} *constrained strain tensor*

$\sigma_m = p$ *mean stress*

σ_s *generalized shear stress*

ε_v *volumetric strain*

ε_s *distortional strain*

$\sigma_1, \sigma_2, \sigma_3$ *major, intermedine and minor principle stress, respectively*

$\varepsilon_1, \varepsilon_2, \varepsilon_3$ *major, intermedine and minor principle strain, respectively*

D_{ijkl}^{b} *elastic modulus of bonded elements*

D_{ijkl}^{f} *tangential elastoplastic modulus of frictional elements*

D_{ijkl}^{fe} *elastic modulus of frictional elements*

K *bulk modulus*

G *shear modulus*

ν^{fe} Poisson ratio of the frictional elements

ϕ *yielding function*

g *plastic potential*

H *Hardening modulus*

Θ, Γ_ϕ *and* Γ_g *hardening parameters*

n *and* w *power numbers varying with the confining pressures*

p_0 *reference confining pressures at zero plastic volumetric strain in drained triaxial compression tests*

$c_c, c_d, \alpha_\phi, \alpha_{\phi 0}, \alpha_g$ *and* α_{g0} *material parameters*

λ *virgin compression slope on* $\varepsilon_v^f - \ln p^f$ *plot*

e_0 *initial void ratio on* $\varepsilon_v^f - \ln p^f$ *plot*

κ *rebounding slope on* $\varepsilon_v^f - \ln p^f$ *plot*

M, Z, Λ_ϕ *and* Λ_g *material constants*

P_a *standard atmospheric pressure*

φ_r *residual angle of inner friction*

N *Number of freeze − thaw cycles*

R_V *breakage ratio*

β, ζ *and* ϖ *material parameters varying with confining pressures*

ψ material constant

A_{ijkl} *local strain coefficient which connects the strain of bonded and frictional elements*

L_{ijkl} *strain coefficient which connects the strain of bonded elements and RVE*

I_{ijkl} *unit tensor*

δ_{ij} *Kronecker delta*

Reference

1. Aubertin, M., Ricard, J.F., and Chapuis, RP. (1999) A predictive model for the water retention curve: application to tailings from hard-rock mines. Canadian Geotechnical Journal, 35(35): 55-69.

2. Beier, N.A., and Sego, D.C. (2009) Cyclic freeze-thaw to enhance the stability of coal tailings. Cold Regions Science and Technology, 55(3): 278-285.

3. Booshehrian, A., Wan, R.., and Su, X. (2019) Hydraulic variations in permafrost due to open-pit mining and climate change: a case study in the Canadian Arctic. Acta Geotechnica, 1-32.

4. Bourgès-Gastaud, S., Dolez, P., Blond, E., and Touze-Foltz, N. (2017) Dewatering of oil sands tailings with an electrokinetic geocomposite. Minerals Engineering, 100: 177-186.

5. Cai, L., Ma, B., Li, X., Lv, Y., Liu, Z., and Jian, S. (2016) Mechanical and hydration characteristics of autoclaved aerated concrete (AAC) containing iron-tailings: Effect of content and fineness. Construction and Building Materials, 128: 361-372.

6. Chakraborty, D., and Choudhury, D. (2009) Investigation of the behavior of tailings earthen dam under seismic conditions. American journal of engineering and applied sciences, 2(3): 559-564.

7. Chen, F., Yao, Q., and Tian, J. (2016) Review of ecological restoration technology for mine tailings in China. Engineering Review, 36(2): 115-121.

8. Cheng, W., Cui, H., Ma, Y., and Yang, X. (2017) Effect of freezing and thawing on soil water migration and microscopic study. Low Temperature Architecture Technology (in Chinese), 39(7): 78-81.

9. Cui, H.H., Liu, J.K., Zhang, L.Q., and Tian, Y.H. (2015) A constitutive model of subgrade in a seasonally frozen area with considering freeze-thaw cycles. Rock & Soil Mechanics (in Chinese), 36(8): 2228-2236.

10. Dai, W.T., Wei, H.B., Liu, H.B., and Gao, Y.P. (2007) Dynamic damage model of silty clay after freeze-thaw cycles. Journal of Jilin University (in Chinese), 37(4): 790-793.

11. Dan, C., Liu, J., and Xu, L.I. (2016) A constitutive model with double yielding surfaces for silty sand

after freeze-thaw cycles. Chinese Journal of Rock Mechanics & Engineering, 35(3): 623-630.

12. Davies, M.P., McRoberts, E.C., and Martin, T.E. (2002) Static liquefaction of tailings–fundamentals and case histories. In Proceedings, Tailings Dams 2002. ASDSO/USCOLD, Las Vegas.

13. Eshelby, J.D. (1957) The determination of the elastic field of an ellipsoidal inclusion, and related problems. Proc. R. Soc. Lond. A, 241(1226): 376-396.

14. Eshelby, J.D. (1959) The elastic field outside an ellipsoidal inclusion. Proc. R. Soc. Lond. A, 252(1271): 561-569.

15. Harlan, R.L. (1973) Analysis of Coupled Heat-Fluid Transport in Partially Frozen Soil. Water Resources Research, 9(5): 1314-1323.

16. Hu, L., Wu, H., Zhang, L., Zhang, P., and Wen, Q. (2016) Geotechnical Properties of Mine Tailings. Journal of Materials in Civil Engineering, 29(2): 04016220.

17. Hu, T., Liu, J., Wang, T.L., and Yue, Z. (2018) Effect of freeze-thaw cycles on the deformation characteristics of a silty clay and its constitutive model with double yielding surfaces. Rock and Soil Mechanics (in Chinese), 40(3): 1-11.

18. Hu, T., Liu, J., Chang, D., Fang, J., and Xu, A. (2018) Influence of freeze-thaw cycling on mechanical properties of silty clay and Ducan-Chang constitutive model. China Journal of Highway and transport (in Chinese), 31(2): 298-307.

19. Lambe, T.W. (1960) A mechanistic picture of shear strength in clay. Proc.asce Research Conf.on Shear Strength of Conhesive Soils, 437(3): 555-580.

20. Liu, E.L., Yu, H.S., Zhou, C., Nie, Q., and Luo, K.-T. (2017) A binary-medium constitutive model for artificially structured soils based on the disturbed state concept and homogenization theory. International Journal of Geomechanics, 17(7): 04016154.

21. Liu, E.L., and Xing, H.L. (2009) A double hardening thermo-mechanical constitutive model for overconsolidated clays. Acta Geotechnica, 4(1): 1-6.

22. Liu, J., Chang, D., and Yu, Q. (2016) Influence of freeze-thaw cycles on mechanical properties of a silty sand. Engineering Geology, 210: 23-32.

23. Liu, Q., Wang, Z. Li, Z., and Wang, Y. (2019) Transversely isotropic frost heave modeling with heat–moisture–deformation coupling. Acta Geotechnica, 1-15.

24. Liu, Y., Huang, R., Liu, E., and Hou, F. (2018) Mechanical behaviour and constitutive model of tailing soils subjected to freeze-thaw cycles. European Journal of Environmental and Civil Engineering: 1-23.

25. Loch, J.P.G. and Kay, B.D. (1978) Water redistribution in partially frozen, saturated silt under several temperature gradients and overburden loads1. Soil Science Society of America Journal, 42(3): 400-406.

26. Mori, T., and Tanaka, K. (1973) Average stress in matrix and average elastic energy of materials with misfitting inclusions. Acta Metallurgica, 21(5): 571-574.

27. Naeini, M., and Akhtarpour, A. (2018) Numerical analysis of seismic stability of a high centerline tailings dam. Soil Dynamics and Earthquake Engineering, 107: 179-194.

28. Nimbalkar, S., Annapareddy, V.S.R., and Pain, A. (2018) A simplified approach to assess seismic stability of tailings dams. Journal of Rock Mechanics and Geotechnical Engineering, 10(6): 1082-1090.

29. Nmai, C.K., 2006. Freezing and thawing. In: Lamond, J.F., Pielert, J.H. (Eds.), Significance of Tests and Properties of Concrete and Concrete Making. American Society for Testing and Materials, Philadelphia.

30. Peng, X., Tang, S., Hu, N., and Han, J. (2016) Determination of the Eshelby tensor in mean-field schemes for evaluation of mechanical properties of elastoplastic composites. International Journal of Plasticity, 76: 147-165.

31. Proskin, S., Sego, D., and Alostaz, M. (2010) Freeze-thaw and consolidation tests on Suncor mature fine tailings (MFT). Cold Regions Science and Technology, 63(3): 110-120.

32. Rassam, D.W., and Williams, D.J. (1999) Unsaturated hydraulic conductivity of mine tailings under wetting and drying conditions. Geotechnical Testing Journal, 22(2): 138-146.

33. Rempel, A.W., 2007. Formation of ice lenses and frost heave. Journal of Geophysical Research: Earth Surface, 112(F2).

34. Shen, Z.J. (2006) Progress in binary medium modeling of geological materials. In Modern Trends in Geomechanics. Springer. pp. 77-99.

35. Shen, Z. (1995) A Double Hardening Model for Clays. Rock and Soil Mechanics (in Chinese), 16(1): 1-8.

36. Shen, Z. (2002) Breakage mechanics and double-medium model for geological materials. Hydro-Science and Engineering (in Chinese), 27(4): 1-6.

37. Stanczyk, M.H., Feld, I.L., and Collins, E.W. (1971) Dewatering Florida phosphate pebble rock slime by freezing techniques. Ntis Pb.

38. Wang, D.Y., Ma, W., Niu, Y.H., Chang, X.X., and Wen, Z. (2007) Effects of cyclic freezing and thawing on mechanical properties of Qinghai–Tibet clay. Cold Regions Science & Technology, 48(1): 34-43.

39. Wang, D.Y., Wei, M.A., Chang, X.X., Sun, Z.Z., Feng, W.J., and Zhang, J.W. (2005) Physico-mechanical properties changes of Qinghai-Tibet clay due to cyclic freezing and thawing. Chinese

Journal of Rock Mechanics & Engineering, 24(23): 4313-4319.

40. Wang, J.G., Leung, C.F., and Ichikawa, Y. (2002) A simplified homogenisation method for composite soils. Computers and Geotechnics, 29(6): 477-500.

41. Wang, S., Liu, F., and Jilin, Q.I. (2016) Statistical damage constitutive model for silty clay after freeze-thaw cycling. Journal of Northwest A & F University (in Chinese), 44(12): 226-234.

42. Wei, Z.A., Yang, Y.H., Jia-Jun, X.U., and Chen, Y.L. (2016) Experimental study on the mechanical properties of frozen tailings by uniaxial compression tests. Journal of Northeastern University (in Chinese), 31(1): 124-142.

43. Wijewickreme, D., Sanin, M.V., and Greenaway, G.R. (2005) Cyclic shear response of fine-grained mine tailings. Canadian Geotechnical Journal, 42(5): 1408-1421.

44. Xu, X., Xu, Y., Chen, G., and Yu, X. (2004) Testing study on engineering characteristics of phosphogypsum. Chinese Journal of Rock Mechanics and Engineering, 12: 031.

45. Yin, G., Zhang, Q., Wang, W., Chen, Y., Geng, W., and Liu, H. (2012) Experimental study on the mechanism effect of seepage on microstructure of tailings. Safety Science, 50(4): 792-796.

46. Lu, Y., Liu, S., Alonso, E., Wang, L., Xu, L. and Li, Z., 2019. Volume changes and mechanical degradation of a compacted expansive soil under freeze-thaw cycles. Cold Regions Science and Technology, 157, pp.206-214.

47. Zhang, C., and Liu, Z. (2018) Freezing of water confined in porous materials: role of adsorption and unfreezable threshold. Acta Geotechnica, 13: 1203-1213.

48. Zhang, D. and Liu, E. (2019) Binary-medium-based constitutive model of frozen soils subjected to triaxial loading. Results in Physics, 12**:** 1999-2008.

49. Zhang, M., Zhang, X., Lai, Y., Lu, J., and Wang, C. (2018) Variations of the temperatures and

volumetric unfrozen water contents of fine-grained soils during a freezing–thawing process. Acta Geotechnica, 1-7.

50. Zhang, Q., Yin, G., Wei, Z., Fan, X., Wang, W., and Nie, W. (2015) An experimental study of the mechanical features of layered structures in dam tailings from macroscopic and microscopic points of view. Engineering Geology, 195: 142-154.

51. Zhang, Z., Wei, M.A., Feng, W., Xiao, D., and Hou, X. (2016) Reconstruction of Soil Particle Composition During Freeze-Thaw Cycling:A Review. Pedosphere, 26(2): 167-179.

List of Figures:

Fig. 1 Sketch of binary-medium model.

Fig. 2 Components of shear resistance:

(a) Strain-softening behavior;

(b) Strain-hardening behavior.

Fig. 3 Structure model of tailing soils.

Fig. 4 Four types of RVE of tailing soils:

(a) Frictional-elements RVE;

(b) Reference RVE;

(c) Frictional-elements RVE included single elastic bonded element;

(d) Frictional-elements RVE included elastic bonded elements.

Fig. 5 Comparison between yield surface and potential surface of the double hardening model.

Fig. 6 The evolution of breakage ratio R_V versus distortional strain ε_s under various material parameters:

(a) The influence of material parameters β;

(b) The influence of material parameters ζ;

(c) The influence of material parameters ϖ.

Fig. 7 The influence of freezing-thawing cycles on the weight and volume variation of tailing soils.

(a) The weight variation

(b) The volume variation

Fig. 8 The variation of parameters of bonded elements with freeze-thaw cycles *N*:

(a) The elastic bulk modulus K^b;

(b) The shear modulus G^b.

Fig. 9 Drained triaxial test results of frictional tailing soils samples:

(a) The generalized shear stress–distortional strain curves;

(b) The volumetric strain–distortional strain curves.

Fig. 10 Comparisons between predicted and tested results:

(a) The generalized shear stress–distortional strain curves;

(b) The volumetric strain–distortional strain curves.

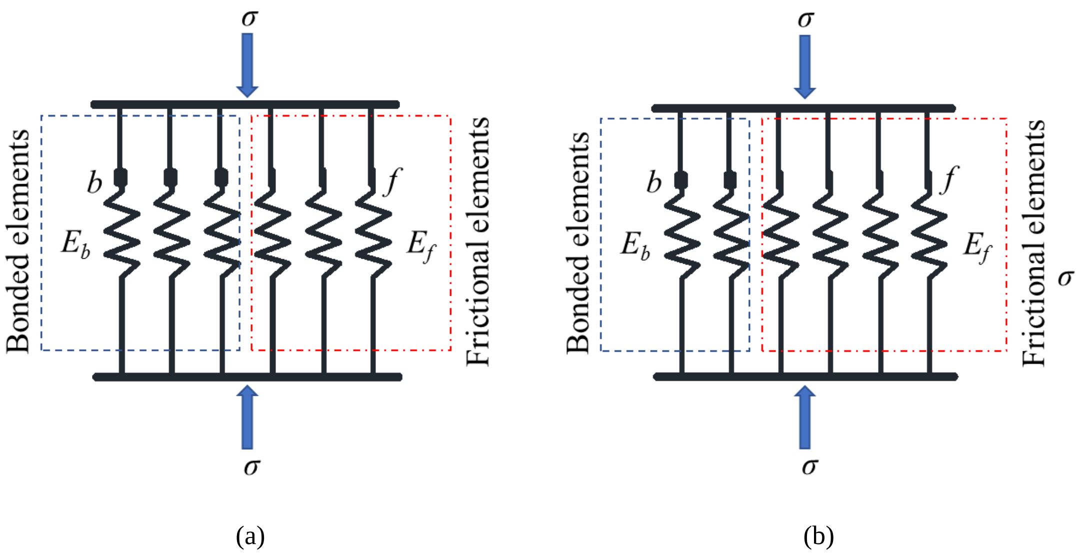

Fig. 1 Sketch of binary-medium structure

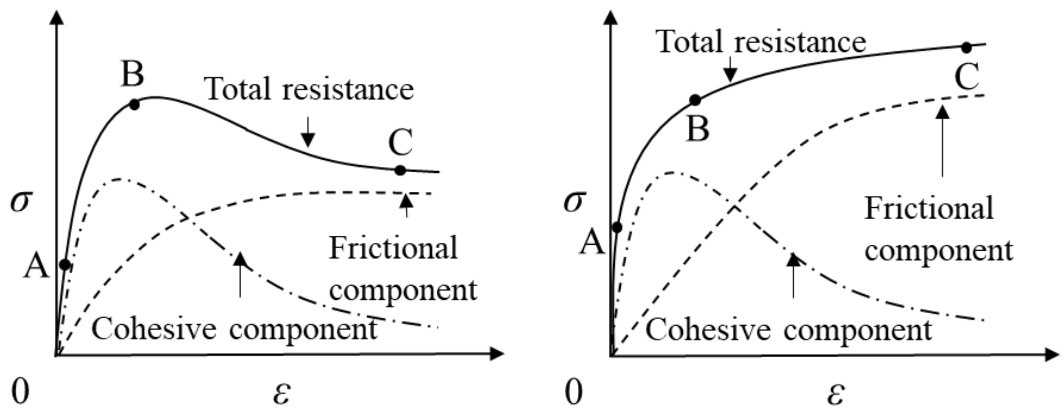

(a) Strain-softening behavior (b) Strain-hardening behavior

Fig. 2 Components of shear resistance

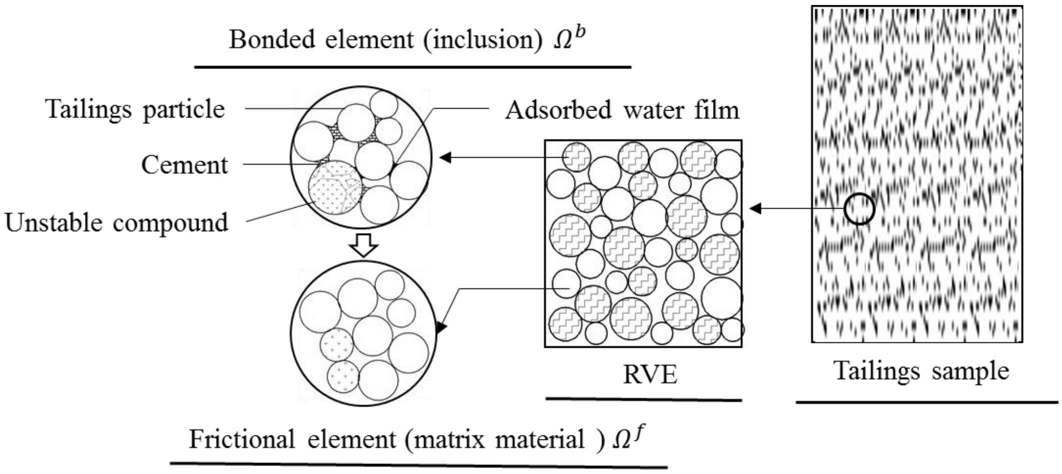

Fig. 3 Structure model of tailing soils

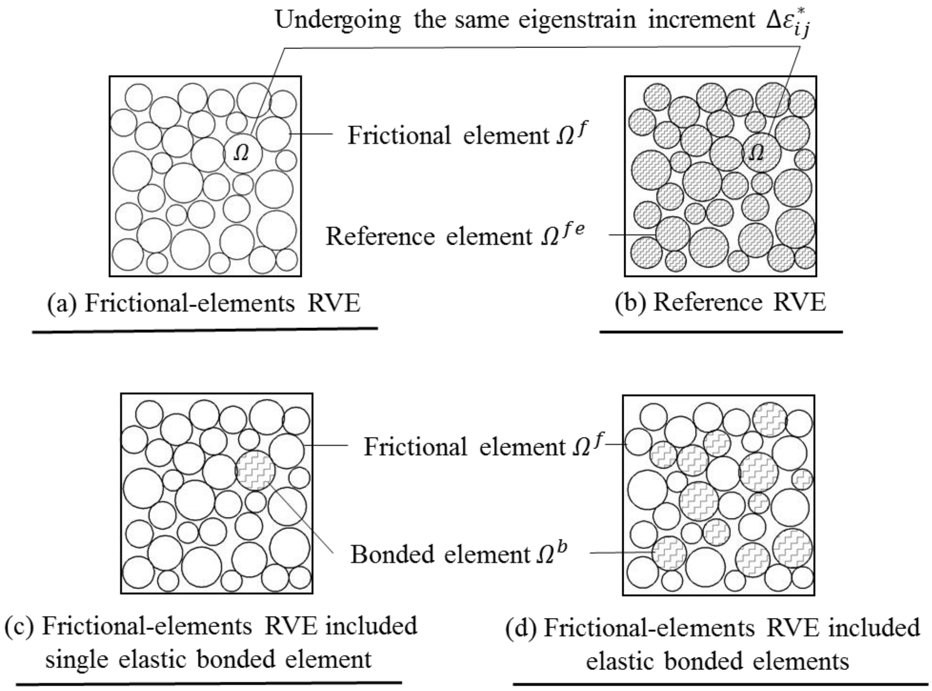

Fig. 4 Four types of RVE of tailing soils

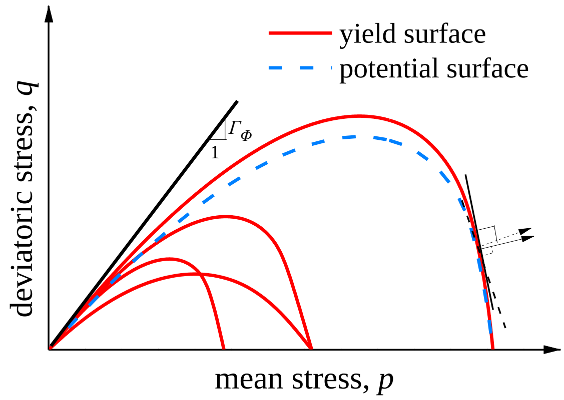

Fig. 5 Comparison between yield surface and potential surface of the double hardening model

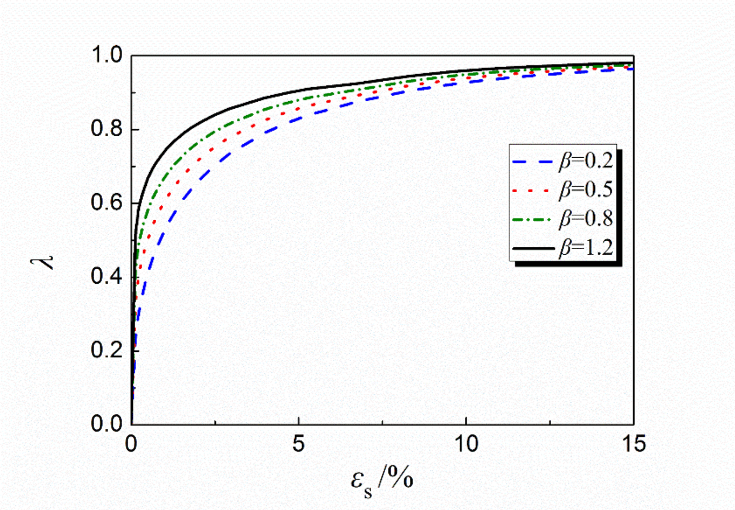

(a) The influence of material parameters β

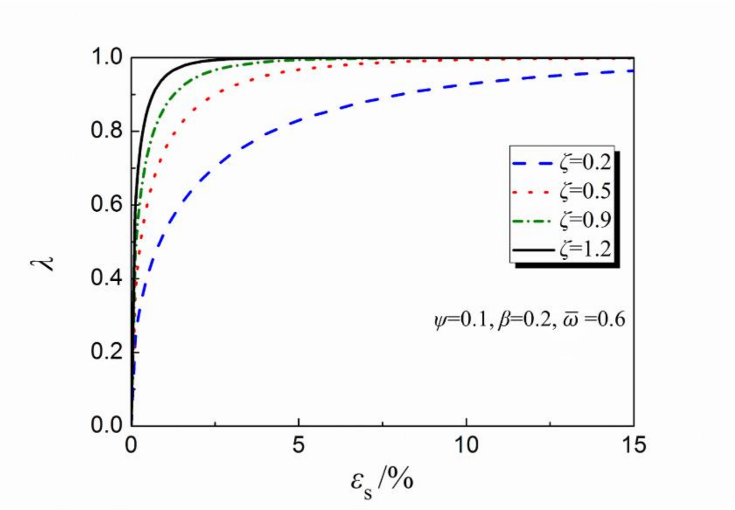

(b) The influence of material parameters ζ

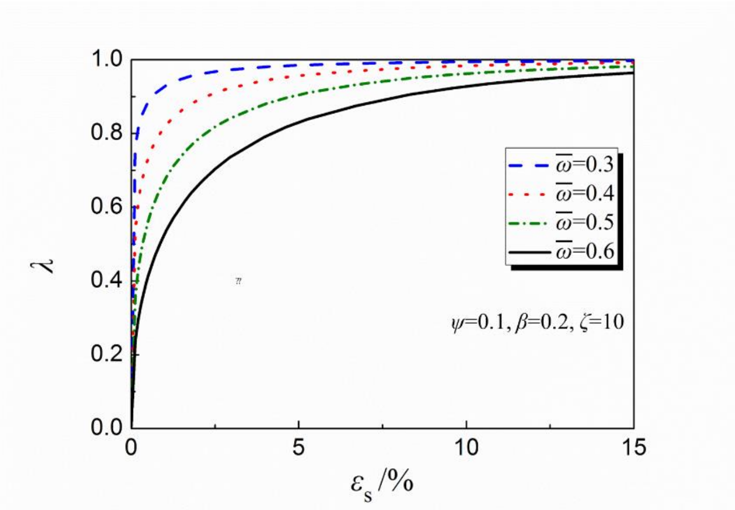

(c) The influence of material parameters ϖ

Fig. 6 The evolution of breakage ratio R_V versus distortional strain ε_s under various material parameters

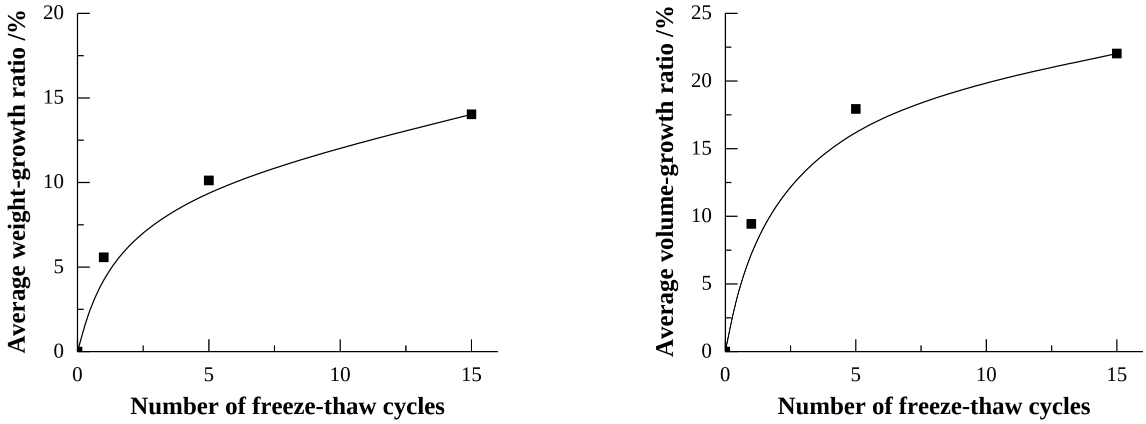

(a) The weight variation (b) The volume variation

Fig. 7 The influence of freezing-thawing cycles on the weight and volume variation of tailing soils

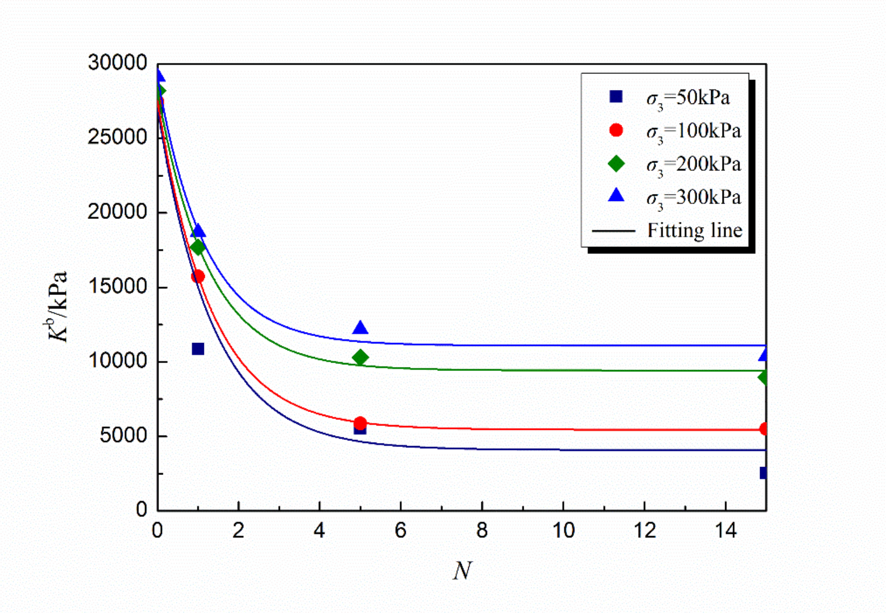

(a) The elastic bulk modulus K^b

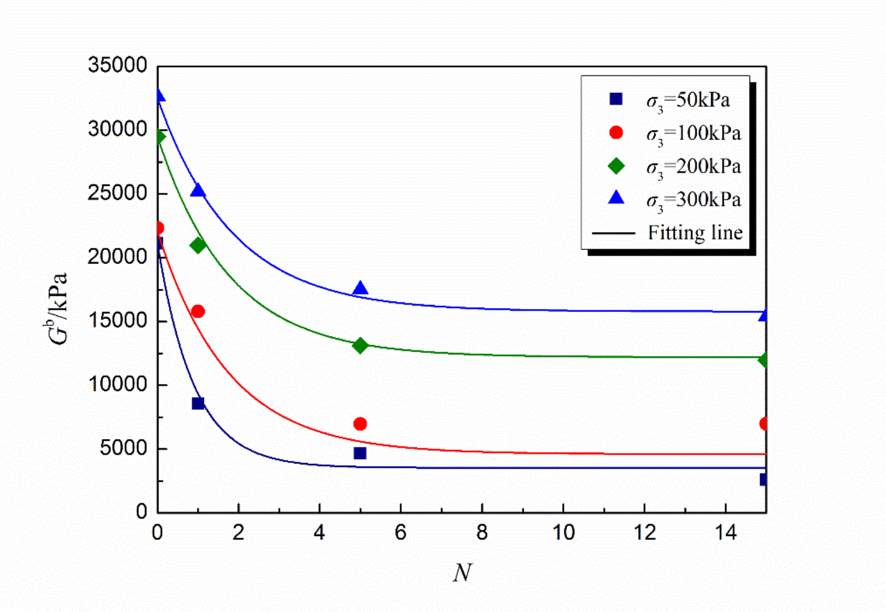

(b) The shear modulus G^b

Fig. 8 The variation of parameters of bonded elements with freeze-thaw cycles N

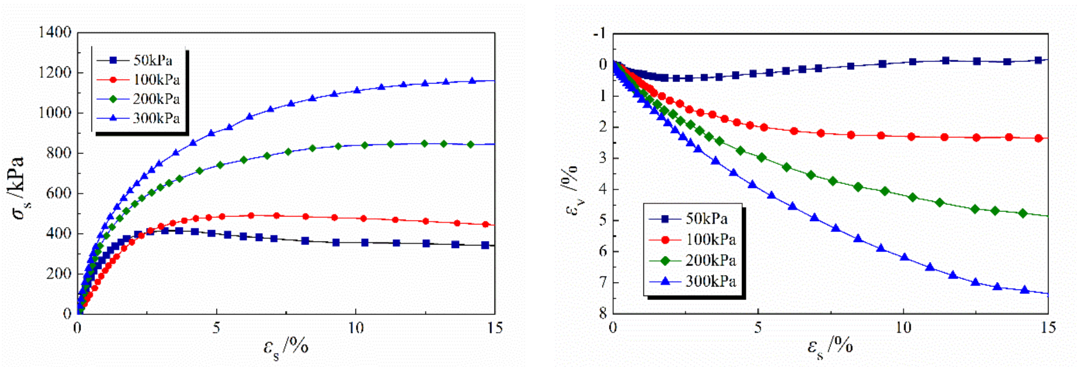

(a) The generalized shear stress –distortional strain curves

(b) The volumetric strain –distortional strain curves

Fig. 9 Drained triaxial test results of frictional tailing soils samples.

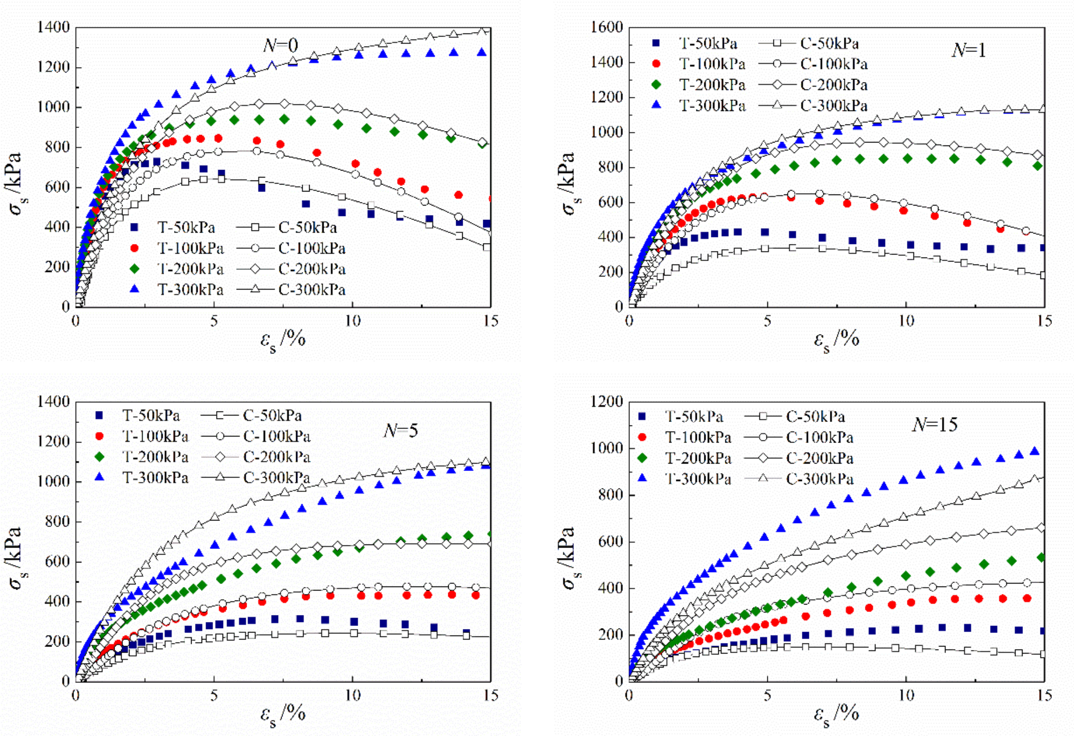

(a) The generalized shear stress–distortional strain curves

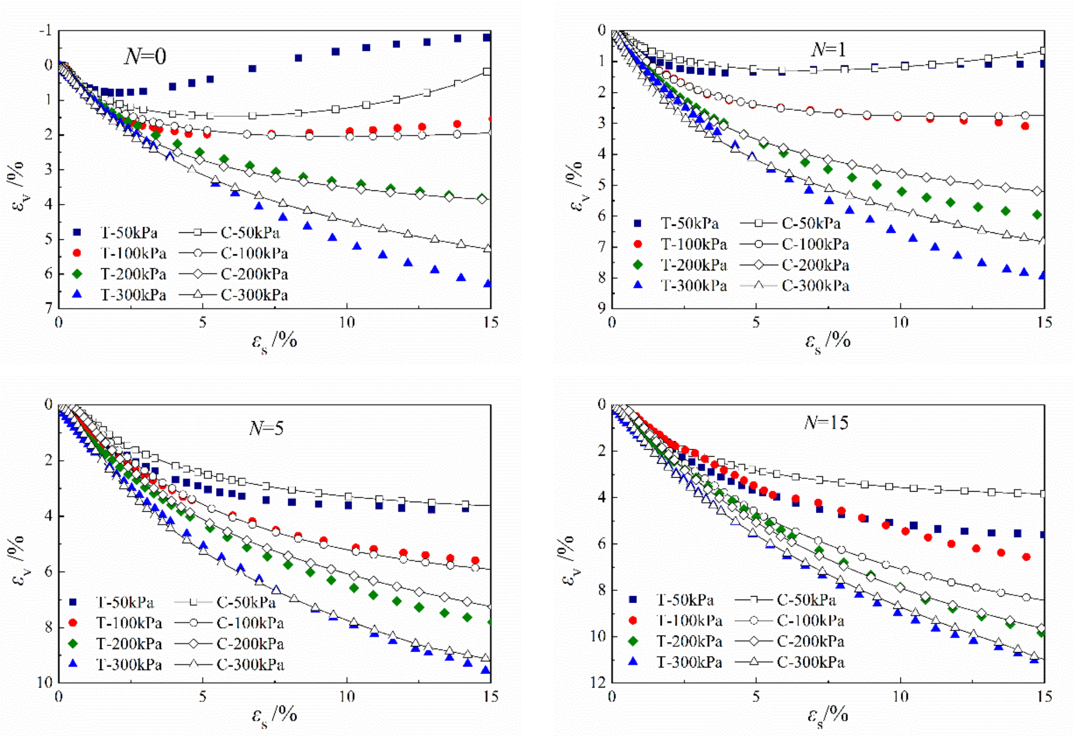

(b) The volumetric strain–distortional strain curves

Fig. 10 Comparisons between predicted and tested results.